Ann. Geophys., 29, 1401–1410, 2011
www.ann-geophys.net/29/1401/2011/
doi:10.5194/angeo-29-1401-2011


Annales Geophysicae

# Statistical characteristics of gravity wave activities observed by an OH airglow imager at Xinglong, in northern China

**Q. Li[1,2], J. Xu[1], J. Yue[3], W. Yuan[1,2], and X. Liu[1,4]**

[1]State Key Laboratory of Space Weather, Center for Space Science and Applied Research, Chinese Academy of Sciences, Beijing 100190, China
[2]Graduate University of the Chinese Academy of Sciences, Beijing 100049, China
[3]High Altitude Observatory, National Center for Atmospheric Research, Boulder, CO 80307, USA
[4]College of Mathematics and Information Science, Henan Normal University, Xinxiang, China

Received: 24 May 2011 – Revised: 26 July 2011 – Accepted: 4 August 2011 – Published: 23 August 2011

**Abstract.** An all-sky airglow imager (ASAI) was installed at Xinglong, in northern China (40.2° N, 117.4° E) in November 2009 to study the morphology of atmospheric gravity waves (AGWs) in the mesosphere and lower thermosphere (MLT) region. Using one year of OH airglow imager data from December 2009 to November 2010, the characteristics of short-period AGWs are investigated and a yearlong AGW climatology in northern China is first ever reported. AGW occurrence frequency in summer and winter is higher than that in equinoctial months. Observed bands mainly have horizontal wavelengths from 10 to 35 km, observed periods from 4 to 14 min and observed horizontal phase speeds in the range of 30 to 60 m s$^{-1}$. Most of the bands propagate in the meridional direction. The propagation directions of the bands show a strong southwestward preference in winter, while almost all bands propagate northeastward in summer. Although the wind filtering in the middle atmosphere may control AGW propagations in the zonal direction, the non-uniform distribution of wave sources in the lower atmosphere may contribute to the anisotropy in the meridional direction in different seasons. Additionally, as an indication of local instability, the characteristics of ripples are also analyzed. It also shows seasonal variations, occurring more often in summer and winter and mainly moving westward in summer and eastward in winter.

**Keywords.** Atmospheric composition and structure (Airglow and aurora) – Meteorology and atmospheric dynamics (Middle atmosphere dynamics; Waves and tides)

*Correspondence to:* Q. Li
(qzli@spaceweather.ac.cn)

## 1 Introduction

The atmospheric gravity wave (AGW) is an important atmospheric phenomenon (Hines, 1960). They are mainly generated in the troposphere by convection, front/jet stream, orography and other sources. Although the middle atmosphere wind filtering would block some of the upward propagation of AGWs, some fast propagating AGWs can reach the mesosphere and lower thermosphere (MLT) region. To conserve the wave energy, the amplitude of the AGWs becomes large and leads to wave saturation and breaking, influencing the balance of dynamics and thermodynamics in the MLT (Vincent, 1984; Taylor et al., 2001; Fritts and Alexander, 2003, and references therein). Therefore, AGWs play an important role in momentum and energy transports, thus controlling the global-scale circulation in the MLT region (Houghton, 1978; Lindzen, 1981; Holton, 1982). Hence, the studies of AGWs and their effects in the MLT have been one of the essential topics of the upper atmosphere dynamics (Fritts and Alexander, 2003).

There are many techniques to observe the gravity wave activities in the middle and upper atmosphere, such as radars, lidars, photometers, rockets and satellite observations. In particular, airglow imaging technique developed in 1970s (Peterson and Kieffaber, 1973) provides a unique detecting method by monitoring the nighttime airglow emission perturbation induced by the AGWs. Since then, many investigators have studied the two-dimensional horizontal characteristics of AGWs in the MLT region using imaging technique (Taylor, 1997). Through image processing, we can retrieve AGW propagation directions, horizontal wavelengths, apparent phase velocities and apparent periods.

Published by Copernicus Publications on behalf of the European Geosciences Union.

Seasonal variations of gravity wave activities in the MLT region have been studied by several investigators with all-sky imagers (e.g., Wu and Killeen, 1996; Nakamura et al., 1999; Walterscheid et al., 1999; Medeiros et al., 2003; Ejiri et al., 2003; Kim et al., 2010) over the past decades. Wu and Killeen (1996) found that the gravity wave activities from OH airglow observations showed a maximum in summer and much weaker activities in winter at the Peach Mountain Observatory, Michigan (42.3° N, 83.7° W) from 1993 to 1994. From 18 months of OH imager observations at Shigaraki (34.9° N, 136.1° E), Nakamura et al. (1999) reported AGWs propagated eastward in summer and westward in winter, respectively. Using one year OH Meinel and OI (557.7 nm) band image data at Rikubetsu (43.5° N, 143.8° E) and Shigaraki (34.9° N, 136.1° E) in Japan from October 1998 to October 1999, Ejiri et al. (2003) reported that AGWs propagated either northward or northeastward in summer at both sites. However, AGWs propagated generally westward at Rikubetsu and dominantly southwestward at Shigaraki in winter. By using long-term OH Meinel, $O_2$ and OI (557.7 nm) band image data from July 2001 to September 2005 at Mt. Bohyun, Korea (36.2° N, 128.9° E), Kim et al. (2010) found that AGWs showed preference propagation directions, propagating westward during fall and winter, and eastward during spring and summer. In the Southern Hemisphere, by using OH Meinel and $O_2$ band image data from April 1995 to January 1996 in Adelaide (35° S, 138° E), Australia, Walterscheid et al. (1999) presented that most gravity waves were possibly thermally ducted, mainly propagating poleward in summer and equatorward in winter. Medeiros et al. (2003), by analyzing 12 months observation at Cachoeira Paulista (23° S, 45° W), found gravity waves exhibited preference propagation directions, propagating southeast in summer and northwest in winter.

The wave structures recorded by airglow imagers are usually short-period AGWs (<1 h) with small horizontal wavelengths (from 5 to 100 km) and long enough vertical wavelengths (>10 km) (Liu and Swenson, 2003). Although some special waves, such as "bores" and "walls", can be observed by the airglow imagers sometimes (Taylor et al., 1995b; Swenson et al., 1998), most wave patterns are categorized into two types: "bands" and "ripples" (Taylor et al., 1995a, 1997). Bands are large-scale, long-lived and often extended over the entire field of view. These AGWs can propagate freely or be ducted by thermal and/or wind ducts in the MLT (Isler et al., 1997; Walterscheid et al., 1999; Hecht et al., 2001b; Snively and Pasko, 2005). Ripples are short-scale, localized, small spatial extent ($< 5 \times 10^3$ km$^2$) and exhibit short lifetime (<45 min) (Peterson, 1979). They are believed to be generated in-situ likely owing to dynamical or convective instabilities (Hecht et al., 2001a; Hecht, 2004; Li et al., 2005a, b; Yue et al., 2010).

In this paper, we study the characteristics of wave patterns, including both bands and ripples, observed by the all-sky airglow imager (ASAI) of near infrared (NIR) hydroxyl (OH) Meinel bands around 87 km height at Xinglong (40.2° N, 117.4° E), China, from December 2009 to November 2010. The occurrence frequency of AGW structures and seasonal variations of the gravity wave parameters are analyzed. We focus on the seasonal variations of gravity wave propagation directions. In addition, the characteristics of ripples and its seasonal variability are also discussed.

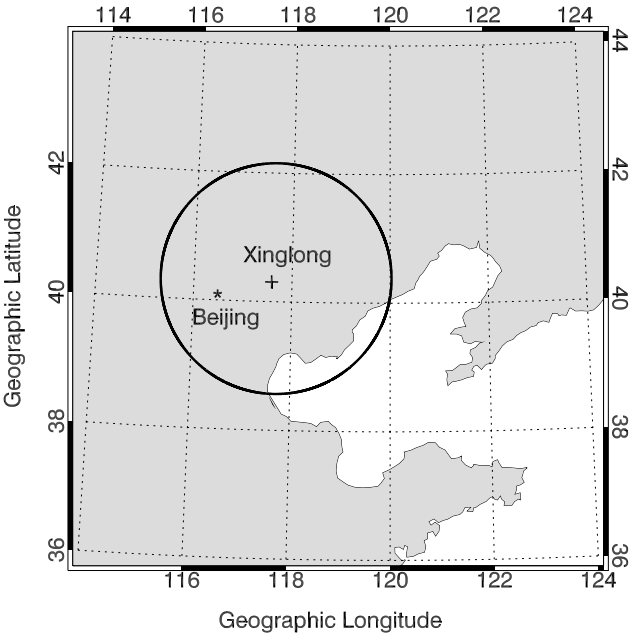


**Fig. 1.** Map showing the location of the all-sky airglow imager at Xinglong (40.2° N, 117.4° E). The circle has a radius of 200 km, which corresponds to a zenith angle of 67° for a height of 87 km.

## 2 Instrumentation and data analysis

An ASAI was deployed at Xinglong (40.2° N, 117.4° E), Hebei Province, in November, 2009 to observe AGWs in the MLT region. Figure 1 shows the location of this imager. The ASAI is part of the Meridian Project (Wang, 2010) optical ground-based instruments. The imager uses a Mamiya 24 mm/f4.0 fisheye lens with a 180° field of view. It is consisted of an eight-position, temperature stabilized filter wheel. The CCD detector is back-illuminated, consisting of $1024 \times 1024$ pixels with a pixel depth of 16 bits. The physical dimension of the CCD array is $13.3 \times 13.3$ mm. The camera system is thermoelectrically cooled to $-70$ °C (dark current <0.5 electrons/pixel/sec). The observation process is controlled automatically by software. In the current study, we only observe the OH Band emission ($87 \pm 5$ km) and do not rotate the filter wheel. A band pass filter of 715–930 nm is inserted for the OH band, with a notch at 865.5 nm to suppress the $O_2$ (0, $-1$) emission. The integration time of OH images is 1 min.

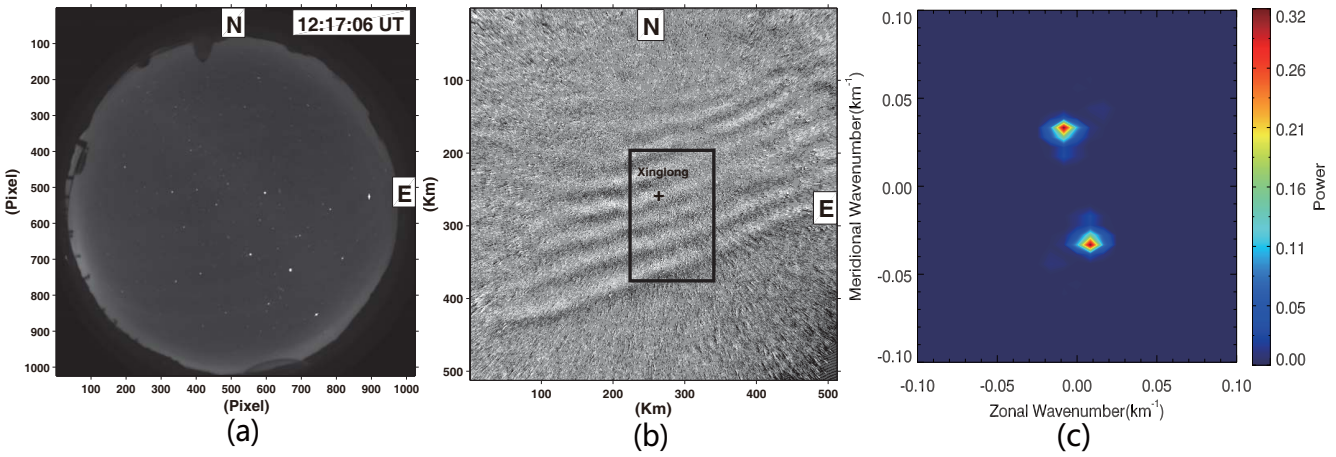


**Fig. 2. (a)** A $1024 \times 1024$ pixels OH airglow raw image observed on the night of 15 January 2010 at 12:17 UT (20:17 LT), **(b)** an unwrapped TD image corresponding in an area of $512 \times 512$ km, **(c)** the power spectrum of the rectangular area ($120 \times 180$ km) in Fig. 2b.

To extract the wave parameters from the airglow images, the raw image data are processed as below. Firstly, we remove the star contaminations with a median filter (Coble et al., 1998; Suzuki et al., 2007; Yue et al., 2009) because the starlight can cause streaking when an image is projected onto geographic coordinates and obscure the wave motions. When the value difference between the raw pixel value and the median of the surrounding pixels exceeds a certain threshold, then the raw pixel value will be replaced by the median value. Secondly, in order to remove the van Rhijin effect and atmospheric extinction in the images, we divide the image by a correction factor described by Kubota et al. (2001). To correct the distortion of the raw image by the fisheye lens, we project the raw images onto geographic coordinate with a size of $512 \times 512$ km, by assuming the OH airglow layer at 87 km (Baker and Stair, 1988). Then, time-difference (TD) images are created by taking the difference between two consecutive images (Swenson and Mende, 1994; Tang et al., 2005; Suzuki et al., 2007). Because the TD process eliminates the background, the high-frequency propagating wave structures have a higher contrast than unprocessed raw images. Figure 2a shows an example of an OH airglow raw image observed on the night of 15 January 2010. Figure 2b shows its corresponding unwrapped TD image in an area of $512 \times 512$ km.

The large-scale structures in airglow images, such as low-frequency AGWs, tides, Milky Way and abrupt background change can distort the wave spectrum calculation. To remove this distortion, we take a step of detrending, which involves fitting a plane (constant) to the TD images and then subtracting the plane from the TD images. A 2-D Hanning window is applied to the TD images to minimize the resulted sidelobe leakage.

Finally, we obtain the AGW parameters (propagation directions, horizontal wavelengths, observed periods and observed phase velocities) through 2-D FFT described by Garcia et al. (1997). The propagation directions and horizontal wavelengths are determined from the positions of the peaks in the power spectrum. The observed period is calculated from the phase change of a sequence of images. For example, Fig. 2c gives the power spectrum of a rectangular area (the size of the area) shown in Fig. 2b. The positions of the peaks are at $(\pm 0.0083, \mp 0.0333)\,\mathrm{km}^{-1}$. Based on the analysis above, the band event in Fig. 1 has a horizontal wavelength of 29 km, a phase velocity of $54\,\mathrm{m\,s}^{-1}$ and an observed period of 9 min. Its azimuth angle is 166° (propagating southeast).

## 3 Results and discussion

### 3.1 The characteristics of gravity waves

To start the statistical study of the AGWs observed by the Xinglong imager, we checked the observing weather condition and the occurrence frequency of wave structures (bands and ripples) for each month from December 2009 to November 2010. The monthly distribution of hours with clear and new moon sky and time periods when wave structures are observed are displayed from December 2009 to November 2010 in Fig. 3a. The time with clear sky near Xinglong is significantly longer in winter than in summer because the summer is often rainy in northern China. So the deduced statistics of AGWs in winter is more reliable than in summer. In this paper, the summer and winter include May–August and November–February, respectively, and spring and autumn cover March–April and September–October, respectively. Figure 3b shows the histogram of monthly mean occurrence frequency of AGW structures. Here, the occurrence frequency is defined as the ratio of the hours with observed wave structures to that with clear sky under new moon

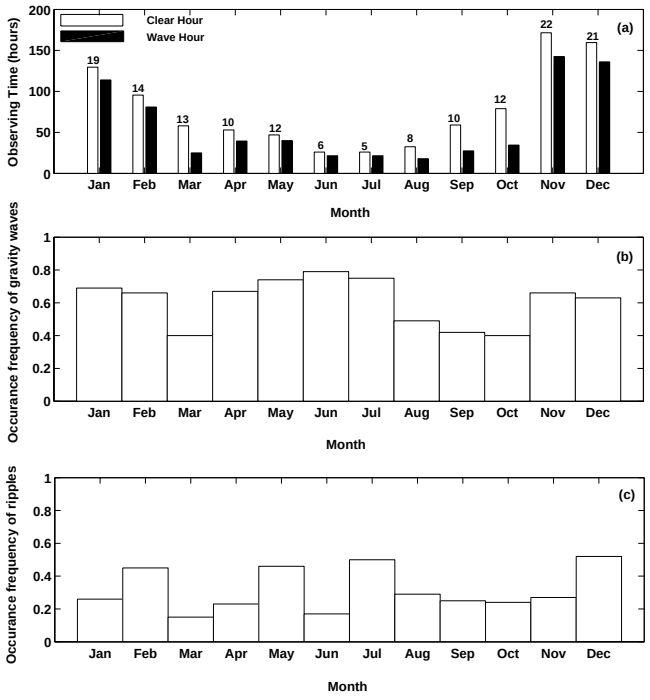


**Fig. 3. (a)** Monthly mean weather condition from December 2009 to November 2010 (open bar), and the monthly mean wave structure (bands and ripples) observing hours (black column). The numbers above bar show the clear sky nights per month, **(b)** occurrence frequency of gravity waves, **(c)** occurrence frequency of ripples.

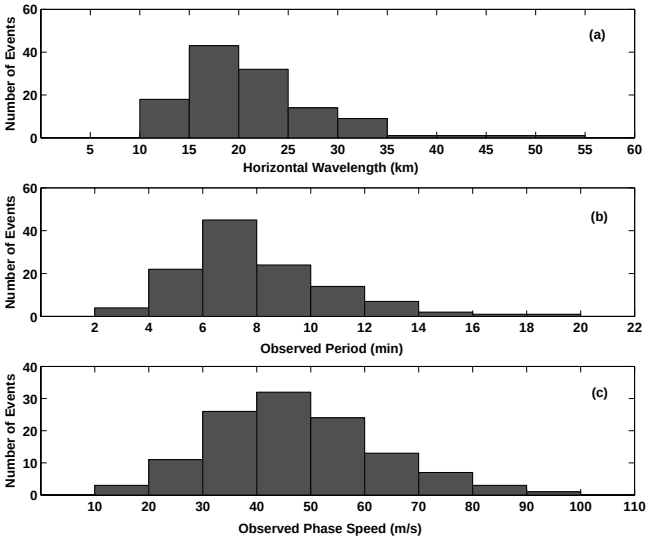


**Fig. 4.** Histograms of band parameters. **(a)** Horizontal wavelength, **(b)** observed wave period, **(c)** observed horizontal phase speed.

condition. The one-year averaged occurrence frequency of wave structures from December 2009 to November 2010 is 75 %. We find that the AGW structures occurrence frequency in summer and winter is higher than that in spring and autumn in Fig. 3b. The wave occurrence frequency in summer may not exactly reflect the feature of wave activities because of the smaller dataset. Nakamura et al. (1999) and Kim et al. (2010) also found the similar seasonal variations with a larger occurrence rate at solstices at Shigaraki (34.9° N, 136.1° E) and Mt. Bohyun, Korea (36.2° N, 128.9° E), respectively. Ejiri et al. (2003) found the AGW occurrence frequency with a slightly value in summer at Rikubetsu (43.5° N, 143.8° E) and Shigaraki (34.9° N, 136.1° E). Dou et al. (2010) reported the AGW occurrence frequency was higher in summer than in other seasons. However, Wu and Killeen (1996) showed most AGWs observed in summer and almost nothing in winter in Michigan (42.3° N, 83.7° W). This discrepancy could be attributed to the fact that Wu and Killeen (1996) only count the AGWs with large perturbation amplitudes ($>7.5$ %) in raw images and AGWs in winter may have smaller amplitudes than in summer. TD images are more sensitive to those AGWs with smaller perturbations.

Figure 4 shows the distributions of the parameters of band events (totally of 120 events). Horizontal wavelengths (Fig. 4a) are in the range of 10–35 km, with an average value of $22 \pm 7$ km (here, 22 is the average value, $\pm 7$ is the standard deviation), observed wave periods (Fig. 4b) are 4–14 min with an average value of $8.1 \pm 3.0$ min. And observed horizontal phase speeds (Fig. 4c) are 30–60 m s$^{-1}$, with an average value of $48 \pm 16$ m s$^{-1}$. Compared to the AGW parameters observed at similar latitudes, Smith et al. (2000) gave similar parameters of band events, with an average horizontal wavelength of $21 \pm 7$ km, an average observed period of $8.5 \pm 4.6$ min, and an average observed horizontal phase speed of $47 \pm 20$ m s$^{-1}$, respectively, at Millstone (42.6° N, 71.5° W). Ejiri et al. (2003) reported an average horizontal wavelength of 21 km from OH airglow images and slightly slower observed horizontal phase speed of 20–50 m s$^{-1}$ from both OH and OI airglow images at Rikubetsu (43.5° N, 143.8° E) and Shigaraki (34.9° N, 136.1° E).

Furthermore, Fig. 5 illustrates the seasonal variations in the averaged parameters of band events. It should be noted that there are no significant seasonal variations of horizontal wavelengths (Fig. 5a). Ejiri et al. (2003) also reported there were no recognizable variations of the average horizontal wavelengths at Rikubetsu (43.5° N, 143.8° E) and Shigaraki (34.9° N, 136.1° E) from both OH and OI airglow images (see the Fig. 6 in Ejiri et al., 2003). Figure 5b indicates larger observed period in summer than in winter. Figure 5c implies smaller observed horizontal phase speed in summer than in winter. However, Ejiri et al. (2003) showed the averaged observed horizontal phase speed was slightly larger in summer than in winter at both locations from OH airglow images. Owing to the smaller dataset in summer, more observation is necessary in summer for a clear picture of the seasonal variations in this area.

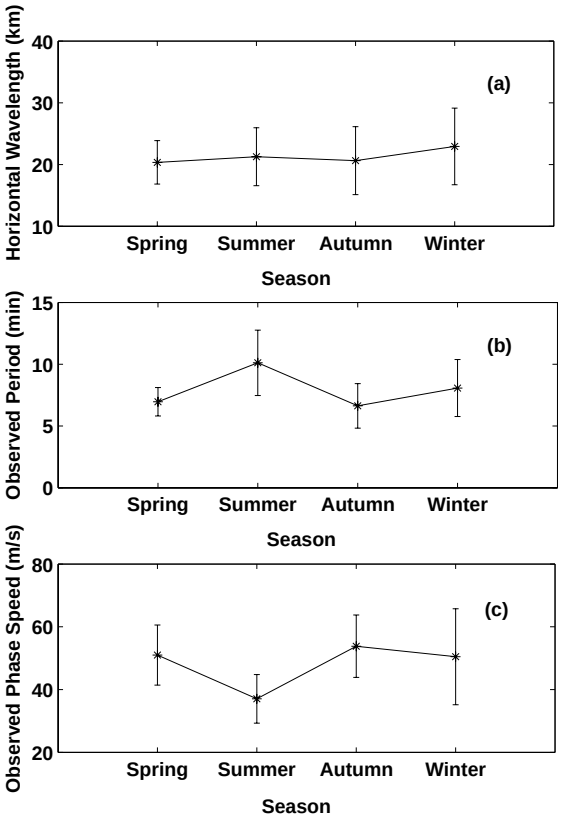


**Fig. 5.** The seasonal variations in the averaged band events parameters. **(a)** Averaged horizontal wavelength, **(b)** averaged observed period, **(c)** averaged horizontal phase speed. Error bars give mean errors for each season.

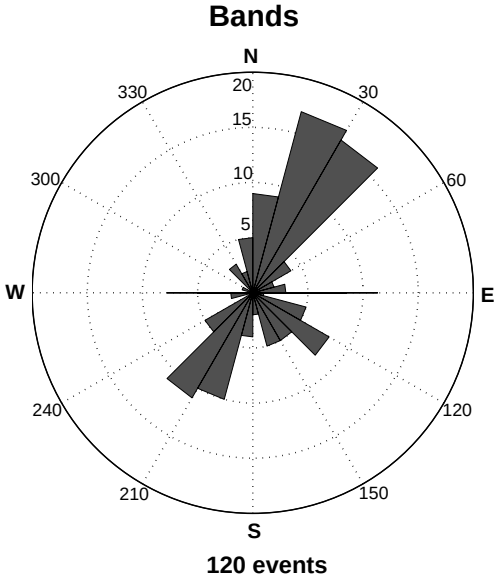


**Fig. 6.** Polar histogram of the propagation directions for all bands. The values in radial direction represent the number of wave propagation in each direction.

### 3.2 Anisotropic propagation direction of bands and its possible mechanisms

Examination on the horizontal propagation direction of AGWs is essential to understand the momentum flux transported by AGWs. The polar histogram of the propagation directions for all bands over one year are given in Fig. 6. Most of bands exhibit dominant propagation in the meridional direction rather than the zonal direction. Figure 7 shows the seasonal variations of the propagation directions of bands. The propagation directions of bands have a strong southwestward preference in winter; on the other hand, almost all bands propagate northeastward in summer. The number of band events in summer is only about half of that in winter, so accumulation of band events in summer with continuing imager observation is necessary to reach a firm conclusion.

Critical-layer filtering effect by the middle atmospheric winds plays an important role in determining the anisotropic distributions of AGW propagation in the zonal direction (Taylor et al., 1993; Medeiros et al., 2003). The AGWs originated from lower atmosphere can be absorbed by the critical-layer where the intrinsic frequency of the wave is Doppler-shifted to zero when they propagate upward. The Doppler-shifted frequency $\Omega$ is expressed as

$$\Omega = \omega - kU, \tag{1}$$

where $\omega$ is the observed angular frequency, $k$ is the horizontal wavenumber, $U$ is the background wind speed in the direction of wave propagation.

Equation (1) can be rewritten as

$$\Omega = \omega(1 - \frac{U}{c}), \tag{2}$$

where $c$ is the observed horizontal phase speed of the wave. Equation (2) can be expressed in terms of the zonal and meridional components of the horizontal wind as

$$\Omega = \omega(1 - \frac{u\cos\theta + v\sin\theta}{c}), \tag{3}$$

where $u$ and $v$ are the zonal and meridional components of the horizontal wind, respectively. $\theta$ is the angle between the horizontal wave vector and the eastward direction. When the AGWs approach a critical-layer where $c \to U$, $\Omega \to 0$, Eq. (3) can be written as

$$c = u\cos\theta + v\sin\theta, \tag{4}$$

using Eq. (4), we can determine the forbidden regions defined by $\Omega \leq 0$, where the AGWs can not survive. The Horizontal Wind Model 07 (HWM-07) (Drob et al., 2008; Emmert et al., 2008) is an empirical model comprising of satellite, rocket and ground-based wind measurements. It is used to estimate the horizontal wind $U$. Figure 8 gives "Blocking diagrams" (e.g., Ryan, 1991; Taylor et al., 1993; Medeiros

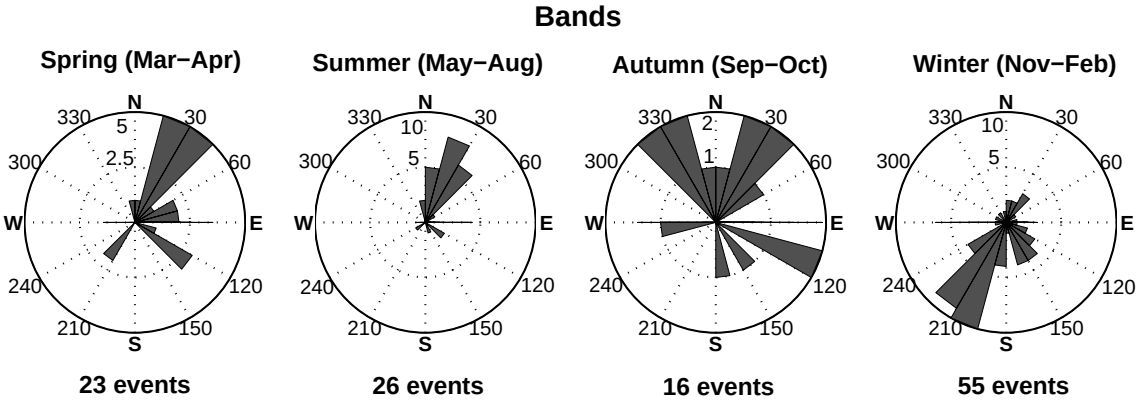


**Fig. 7.** Seasonal variations of the propagation directions of bands.

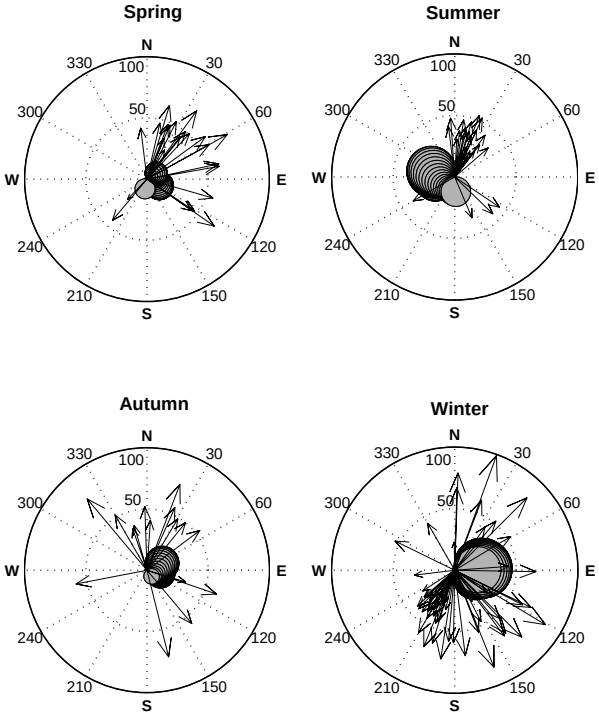


**Fig. 8.** The magnitude (denoted by arrow length) and direction (denoted by arrow direction) of the gravity waves horizontal phase speed during each season. The values in radial direction represent the speed ($m\,s^{-1}$) in each direction. The superimposed area gives "Blocking diagram" for each season from 20 to 85 km height. The wind profiles data for each season from HWM-07 model (averaged from 20:00 to 04:00 LT for each season).

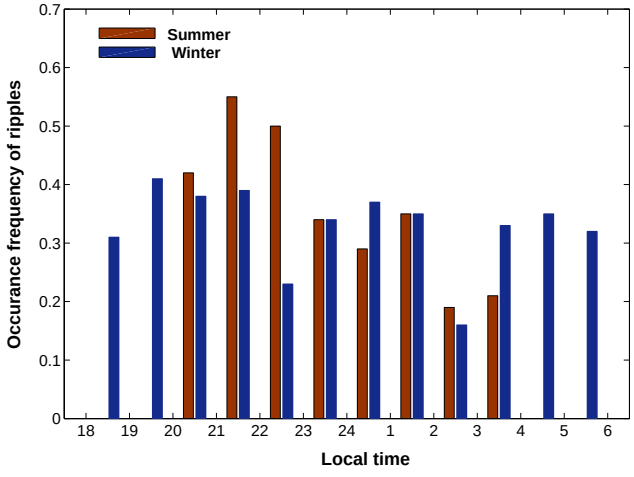


**Fig. 9.** Local time dependence of ripple occurrence frequency in summer and winter.

et al., 2003) and shows the forbidden region for four seasons. The blocking diagram does not match very well with the bands anisotropic distributions. Among the four seasons, summer exhibits a better matching, however, it still can not explain why there is no eastward propagating wave. This may be attributed to the following reasons: (1) the HWM-07 wind may not represent the real wind; (2) critical layer filtering may not be a dominant factor determining the wave directions. As the blocking diagram can partly explain the bands anisotropic distributions, the non-uniform distribution of wave sources and wave ducts may also contribute to the anisotropy of the bands propagation directions in different seasons.

As mentioned, the observed bands mainly propagate southwestward in winter and northeastward in summer. Similarly, from 9 months of airglow imaging observations in Adelaide (35° S, 138° E), Australia, Walterscheid et al. (1999) reported that AGWs dominantly propagated poleward in summer and equatorward in winter. Dou et al. (2010), by analyzing 5 yr of OH imaging observations from September 2003 to September 2008 in Northern Colorado (40.7° N, 104.9° W), reported similar results for the AGW propagation directions in summer and winter. They suggested that the AGWs might be generated from tropical convection regions in summer and from the frontal systems

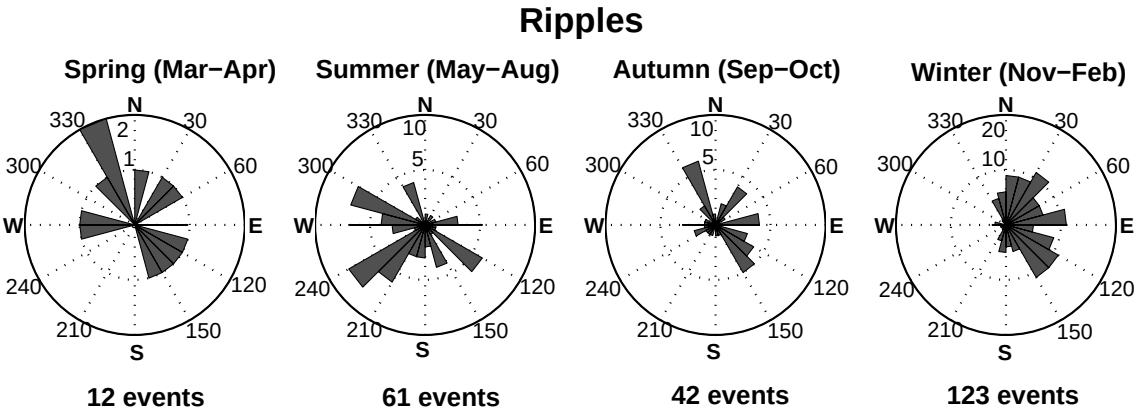


**Fig. 10.** Seasonal variations of the movement directions of ripples.

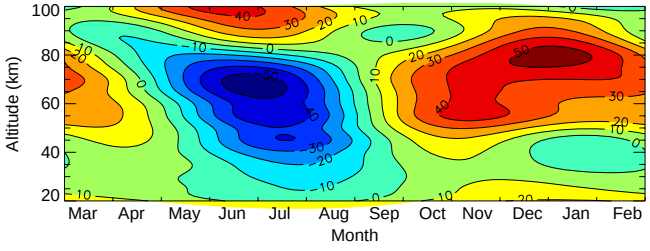


**Fig. 11.** Zonal wind at Xinglong from December 2009 to November 2010 calculated by the HWM-07 model (averaged from 20:00 to 04:00 LT for each month).

at the poleward side of observation sites in winter. To account for the seasonal variation of the AGW propagation in the meridional direction, the non-uniform distribution of wave sources in the lower atmosphere is invoked. Satellite observations (Wu and Waters, 1996; Nakamura et al., 2003) and general circulation modeling (Richter et al., 2010) suggested there are more convection in summer tropical region and more jet stream/frontal systems at winter higher latitudes. Based on multiple years of the Atmosphere Infrared Sounder (AIRS) satellite observations, we do see most of AGWs in the stratosphere propagating away from frontal systems in northern China and Mongolia in winter, and from convection in southern China in summer (L. Hoffmann, personal communication, 2011). Besides the distributions of wave sources, Walterscheid et al. (1999) and Dou et al. (2010) explained that most of AGWs were ducted by the thermal ducts in the lower thermosphere from tropical convection regions in summer. Therefore, our results may be attributed to both the seasonal variations of AGW sources and wave ducts.

Besides the seasonal variations, Dou et al. (2010) also discussed the interannual variations of AGW propagation directions. They found the percentage of propagation in each direction varied from year to year, which may be due to the year-to-year variations of wave sources, thermal ducting regions, and the background wind. In order to understand the climatological properties of AGW propagation, continuous airglow imaging observation covering many years is desired.

### 3.3 The characteristics of ripples

In addition, we also looked at the local instability features, ripples in the Xinglong airglow images. Altogether, we found 238 ripple events from one year of airglow observations. The histogram of monthly mean occurrence frequency of ripples is given in Fig. 3c. It also shows seasonal variations, with higher occurrence frequency in summer (except for June) and winter, and lower in equinoctial months. Moreover, Fig. 9 displays the local time dependence of ripple occurrence frequency in summer and winter. We find that the occurrence frequency of ripples in summer is much larger than that in winter from 22:00 to 23:00 LT, however, it shows larger occurrence frequency of ripples in winter than in summer from 03:00 to 04:00 LT.

The movement directions of ripples are also discussed. Figure 10 shows seasonal variations of the movement direction of ripples. The ripples exhibit predominantly eastward movement directions in winter and westward in summer. However, Nakamura et al. (1999) reported that the movement directions of ripples were preferentially northeastward in summer. We know that once ripples (Kelvin-Helmholtz billows and convective billows) are formed, they move with the mean wind and rotate with the wind shear in the unstable region (Hecht, 2004). Figure 11 shows zonal wind over December 2009 to November 2010 at Xinglong from the HWM-07 Model. The eastward movement of ripples agrees well with the background zonal wind at ∼87 km in winter (see Fig. 11), while the zonal mean wind in summer is close to zero and ripples move westward. A simultaneous background wind measurement would be ideal to reveal the true correlation between the ripple movement directions and background wind directions.

## 4 Summary

In this paper, a yearlong AGW climatology in China is reported for the first time. We study the statistical characteristics of gravity waves observed in the airglow images of NIR OH Meinel bands at Xinglong (40.2° N, 117.4° E) from December 2009 to November 2010. The analysis results are summarized as follows:

1. The occurrence frequency of wave activities in summer and winter is higher than that in equinoctial months.
2. The band events typically have horizontal wavelengths of 10–35 km, observed periods of 4–14 min, and phase speeds of 30–60 m $s^{-1}$.
3. The propagation directions of bands show a strong southwestward preference in winter, almost all waves propagate northeastward in summer.
4. The wind filtering, non-uniform distribution of wave sources and wave ducts may contribute to the anisotropy of the propagation directions in different seasons.
5. The predominantly eastward movement directions for ripples in winter may be due to a strong eastward background wind at 87 km.

It should be noted that the wind data calculated from HWM-07 model may not accurately represent the local wind environment below the airglow layer. In order to investigate in detail the properties of AGWs, simultaneous wind and temperature measurements by other instruments nearby, such as Fabry-Perot interferometer and meteor radar (Jiang et al., 2011), will be included in future work. Through the measurement of airglow intensity perturbation from the power spectrum, we can also estimate the gravity wave momentum flux and its seasonal variability (Swenson and Liu, 1998). This will be addressed in the future.

*Acknowledgements.* We are grateful to Q. Wu for his helpful comments and suggestions. We would also like to thank V. Lakshmi Narayanan for helpful discussion on the data analysis. This research was supported by the National Science Foundation of China (40890165, 40921063, 41074109, 41004063) and the National Important Basic Research Project of China (2011CB811405). This paper was also supported by the Specialized Research Fund for State Key Laboratories. National Center for Atmospheric Research is supported by National Science Foundation. We acknowledge the use of data from the Chinese Meridian Project.

Topical Editor C. Jacobi thanks two anonymous referees for their help in evaluating this paper.

## References

Baker, D. J. and Stair, A. T.: Rocket measurements of the altitude distributions of the hydroxyl airglow, Phys. Scripta, 37, 611–622, 1988.

Coble, M. R., Papen, G. C., and Gardner, C. S.: Computing two-dimensional unambiguous horizontal wavenumber spectra from OH airglow images, IEEE T. Geosci. Remote Sensing, 36, 368–382, 1998.

Dou, X., Li, T., Tang, Y., Yue, J., Nakamura, T., Xue, X., Williams, B. P., and She, C.-Y.: Variability of gravity wave occurrence frequency and propagation direction in the upper mesosphere observed by the OH imager in Northern Colorado, J. Atmos. Sol.-Terr. Phy., 72 , 457–462, 2010.

Drob, D. P., Emmert, J. T., Crowley, G., Picone, J. M., Shepherd, G. G., Skinner, W., Hays, P., Niciejewski, R. J., Larsen, M., She, C.-Y., Meriwether, J. W., Hernandez, G., Jarvis, M. J., Sipler, D. P., Tepley, C. A., O'Brien, M. S., Bowman, J. R., Wu, Q., Murayama, Y., Kawamura, S., Reid, I. M., and Vincent, R. A.: An empirical model of the Earth's horizontal wind fields: HWM07, J. Geophys. Res., 113, A12304, doi:10.1029/2008JA013668, 2008.

Ejiri, M. K., Shiokawa, K., Ogawa, T., Igarashi, K., Nakamura, T., and Tsuda, T.: Statistical study of short-period gravity waves in OH and OI nightglow images at two separated sites, J. Geophys. Res., 108(D21), 4679, doi:10.1029/2002JD002795, 2003.

Emmert, J. T., Drob, D. P., Shepherd, G. G., Hernandez, G., Jarvis, M. J., Meriwether, J. W., Niciejewski, R. J., Sipler, D. P., and Tepley, C. A.: DWM07 global empirical model of upper thermospheric storm-induced disturbance winds, J. Geophys. Res., 113, A11319, doi:10.1029/2008JA013541, 2008.

Fritts, D. C. and Alexander, M. J.: Gravity wave dynamics and effects in the middle atmosphere, Rev. Geophys., 41(1), 1003, doi:10.1029/2001RG000106, 2003.

Garcia, F. J., Taylor, M. J., and Kelley, M. C.: Two-dimensional spectral analysis of mesospheric airglow image data, Appl. Optics, 36(29), 7374–7385, 1997.

Hecht, J. H.: Instability layers and airglow imaging, Rev. Geophys., 42, RG1001, doi:10.1029/2003RG000131, 2004.

Hecht, J. H., Walterscheid, R. L., and Vincent, R. A.: Airglow observations of dynamical (wind shear-induced) instabilities over Adelaide, Australia, associated with atmospheric gravity waves, J. Geophys. Res., 106, 28189–28197, doi:10.1029/2001JD000419, 2001a.

Hecht, J. H., Walterscheid, R. L., Hickey, M. P., and Franke S. J.: Climatology and modeling of quasi-monochromatic atmospheric gravity waves observed over Urbana Illinois, J. Geophys. Res., 106, 5181–5195, doi:10.1029/2000JD900722, 2001b.

Hines, C. O.: Internal atmospheric gravity waves at ionospheric heights, Can. J. Phys., 38, 1441–1481, 1960.

Holton, J. R.: The role of gravity wave induced drag and diffusion in the momentum budget of the mesosphere, J. Atmos. Sci., 39, 791–799, 1982.

Houghton, J. T.: The stratosphere and mesosphere, Q. J. Roy. Meteorol. Soc., 104, 1–29, 1978.

Isler, J. R., Taylor, M. J., and Fritts, D. C.: Observational evidence of wave ducting and evanescence in the mesosphere, J. Geophys. Res., 102(D22), 26301–26313, doi:10.1029/97JD01783, 1997.

Jiang, G., Xu, J., Yuan, W., Ning, B., Wan, W., and Hu, L.: A comparison of mesospheric winds measured by FPI and meteor radar, Sci. China Earth Sci., in review, 2011.

Kim, Y. H., Lee, C., Chung, J. K., Kim, J. H., and Chun, H. Y.: Seasonal Variations of Mesospheric Gravity Waves Observed with an Airglow All-sky Camera at Mt. Bohyun, Korea (36° N), J. Astron. Space Sci., 27(3), 181–188 , doi:10.5140/JASS.2010.27.3.181, 2010.

Kubota, M., Fukunishi, H., and Okano, S.: Characteristics of medium-and large-scale TIDs over Japan derived from OI 630-nm nightglow observation, Earth Planets Space, 53, 741–751, 2001.

Li, F., Liu, A. Z., Swenson, G. R., Hecht, J. H., and Robinson, W. A.: Observations of gravity wave breakdown into ripples associated with dynamical instabilities, J. Geophys. Res., 110, D09S11, doi:10.1029/2004JD004849, 2005a.

Li, T., She, C. Y., Williams, B. P., Yuan, T., Collins, R. L., Kieffaber, L. M., and Peterson, A. W.: Concurrent OH imager and sodium temperature/wind lidar observation of localized ripples over northern Colorado, J. Geophys. Res., 110, D13110, doi:10.1029/2004JD004885, 2005b.

Lindzen, R. S.: Turbulence and stress owing to gravity wave and tidal breakdown, J. Geophys. Res., 86, 9707–9714, 1981.

Liu, A. Z. and Swenson, G. R.: A modeling study of $O_2$ and OH airglow perturbations induced by atmospheric gravity waves, J. Geophys. Res., 108(D4), 4151, doi:10.1029/2002JD002474, 2003.

Medeiros, A. F., Taylor, M. J., Takahashi, H., Batista, P. P., and Gobi, D.: An Investigation of gravity wave activity in the low-latitude upper mesosphere: propagation direction and wind filtering, J. Geophys. Res., 108(D14), 4411–4419, doi:10.1029/2002JD002593, 2003.

Nakamura, T., Higashikawa, A., Tsuda, T., and Matsushita, Y.: Seasonal variations of gravity wave structures in OH airglow with a CCD imager at Shigaraki, Earth Planets Space, 51, 897–906, 1999.

Nakamura, T., Aono, T., Tsuda, T., Admiranto, A. G., Achmad, E., and Suranto: Mesospheric gravity waves over a tropical convective region observed by OH airglow imaging in Indonesia, Geophys. Res. Lett., 30(17), 1882, doi:10.1029/2003GL017619, 2003.

Peterson, A. W.: Airglow events visible to the naked eye, Appl. Optics, 18, 20, 3390–3393, 1979.

Peterson, A. W. and Kieffaber, L. M.: Infrared photography of OH airglow structures, Nature, 242, 321–322, 1973.

Richter, J. H., Sassi, F., and Garcia, R. R.: Toward a Physically Based Gravity Wave Source Parameterization in a General Circulation Model, J. Atmos. Sci., 67, 136–156, 2010.

Ryan, E. H.: Critical layer directional filtering of atmospheric gravity waves: A comparison of airglow and wind profile model, M.S. thesis, Univ. of Cincinnati, Cincinnati, Ohio, 1991.

Smith, S. M., Mendillo, M., Baumgardner, J., and Clark, R. R.: Mesospheric gravity wave imaging at a subauroral site: First results from Millstone Hill, J. Geophys. Res., 105(A12), 27119–27130, doi:10.1029/1999JA000343, 2000.

Snively, J. B. and Pasko, V. P.: Antiphase OH and OI airglow emissions induced by a short- period ducted gravity wave, Geophys. Res. Lett., 32, L08808, doi:10.1029/2004GL022221, 2005.

Suzuki, S., Shiokawa, K., Otsuka,Y. , Ogawa, T., Kubota, M., Tsutsumi, M., Nakamura, T., and Fritts, D. C.: Gravity wave momentum flux in the upper mesosphere derived from OH airglow imaging measurements, Earth Planets Space, 59, 421–428, 2007.

Swenson, G. R. and Liu, A. Z.: A model for calculating acoustic gravity wave energy and momentum flux in the mesosphere from OH airglow, Geophys. Res. Lett., 25(4), 477–480, doi:10.1029/98GL00132, 1998.

Swenson, G. R. and Mende, S. B.: OH emission and gravity waves (including a breaking wave) in all-sky imagery from Bear Lake, UT, Geophys. Res. Lett., 21, 2239–2242, 1994.

Swenson, G. R., Qian, J., Plane, J. M. C., Espy, P. J., Taylor, M. J., Turnbull, D. N., and Lowe, R. P.: Dynamical and chemical aspects of the mesospheric Na "wall" event on October 9, 1993 during the Airborne Lidar and Observations of Hawaiian Airglow (ALOHA) campaign, J. Geophys. Res., 103, 6361–6380, 1998.

Tang, J., Kamalabadi, F., Franke, S. J., Liu, A. Z., and Swenson, G. R.: Estimation of gravity wave momentum flux with spectroscopic imaging, IEEE T. Geosci. Remote Sens., 43, 103–109, 2005.

Taylor, M. J.: A review of advances in imaging techniques for measuring short period gravity waves in the mesosphere and lower thermosphere, Adv. Space Res., 19, 667–676, 1997.

Taylor, M. J., Ryan, E. H., Tuan, T. F., and Edwards, R.: Evidence of preferential directions for gravity wave propagation due to wind filtering in the middle atmosphere, J. Geophys. Res., 98, 6047–6057, 1993.

Taylor, M. J., Bishop, M. B., and Taylor, V.: All-sky measurements of short period waves imaged in the OI (557.7 nm), Na (589.2 nm) and near infrared OH and $O_2$ (0, 1) nightglow emissions during the ALOHA-93 Campaign, Geophys. Res. Lett., 22(20), 2833–2836, doi:10.1029/95GL02946, 1995a.

Taylor, M. J., Turnbull, D. N., and Lowe, R. P.: Spectrometric and imaging measurements of a spectacular gravity wave event observed during the ALOHA-93 campaign, Geophys. Res. Lett., 20, 2849–2852, 1995b.

Taylor, M. J., Pendleton Jr., W. R., Clark, S., Takahashi, H., Gobbi, D., and Goldberg, R. A.: Image measurements of short-period gravity waves at equatorial latitudes, J. Geophys. Res., 102(D22), 26283–26299, doi:10.1029/96JD03515, 1997.

Taylor, M. J., Gardner, L. C., and Pendleton Jr., W. R.: Long-period wave signatures in mesospheric OH Meinel (6, 2) band intensity and rotational Temperature at mid-latitudes, Adv. Space Res., 27, 1171–1179, 2001.

Vincent, R. A.: Gravity-wave motions in the mesosphere, J. Atmos. Terr. Phys., 46, 119–128, 1984.

Walterscheid, R. L., Hecht, J. H., Vincent, R. A., Reid, I. M., Woithe, J., and Hickey, M. P.: Analysis and interpretation of airglow and radar observations of quasi-monochromatic gravity waves in the upper mesosphere and lower thermosphere over Adelaide, Australia (35° S, 138° E), J. Atmos. Sol.-Terr. Phy., 61, 461–478, 1999.

Wang, C.: New Chains of Space Weather Monitoring Stations in China, Adv. Space Res., 8, S08001, doi:10.1029/2010SW000603, 2010.

Wu, D. L. and Waters, J. W.: Satellite observations of atmospheric variances: A possible indication of gravity waves, Geophys. Res. Lett., 23(24), 3631–3634, 1996.

Wu, Q. and Killeen, T. L.: Seasonal dependence of mesospheric gravity waves (<100 Km) at Peach Mountain Observatory,

Michigan, Geophys. Res. Lett., 23(17), 2211–2214, 1996.

Yue, J., She, C.-Y., Nakamura, T., Harrell, S., and Yuan, T.: Mesospheric bore formation from large-scale gravity wave perturbations observed by collocated all-sky OH imager and sodium lidar, J. Atmos. Sol.-Terr. Phy., 72 , 7–18, doi:10.1016/j.jastp.2009.10.002, 2009.

Yue, J., Nakamura, T., She, C.-Y., Weber, M., Lyons, W., and Li, T.: Seasonal and local time variability of ripples from airglow imager observations in US and Japan, Ann. Geophys., 28, 1401–1408, doi:10.5194/angeo-28-1401-2010, 2010.